Copyright by the American Geophysical Union. Stevens, M. H., C. R. Englert, M. T. DeLand, and S. M. Bailey (2007), Polar mesospheric cloud mass and the ice budget: 2. Application to satellite data sets, J. Geophys. Res., 112, D08205, doi:10.1029/2006JD007532.

Polar mesospheric cloud mass and the ice budget: 2. Application to satellite data sets

Michael H. Stevens,[1] Christoph R. Englert,[1] Matthew T. DeLand,[2] and Scott M. Bailey[3]

Received 19 May 2006; revised 19 January 2007; accepted 5 February 2007; published 20 April 2007.

[1] We use satellite observations of mid-UV solar backscattered light from polar mesospheric clouds (PMCs) to constrain the water ice budget. We compare the PMC mass from observations by two instruments: the limb viewing Student Nitric Oxide Explorer (SNOE) and the nadir viewing Solar Backscattered UltraViolet (SBUV) experiments. At 70 ± 2.5°N we find that SNOE measures over three times more PMC mass than the less sensitive SBUV experiment. We directly compare the two data sets by selecting only the brightest 10% of SNOE clouds so that the SNOE and SBUV PMC occurrence frequencies are the same. This comparison shows that the PMC mass averaged over five northern seasons is the same to within uncertainties in the ice particle size distribution. We also find that near midday, the northern SBUV PMC mass is a factor of 2.4 times greater than the southern PMC mass. These results provide new constraints for global climate models of PMC formation.

Citation: Stevens, M. H., C. R. Englert, M. T. DeLand, and S. M. Bailey (2007), Polar mesospheric cloud mass and the ice budget: 2. Application to satellite data sets, *J. Geophys. Res.*, *112*, D08205, doi:10.1029/2006JD007532.

1. Introduction

[2] Polar mesospheric clouds (PMCs) typically appear at high latitudes during the summer. They form at extremely high altitudes (~83 km) in the coldest region of the Earth's atmosphere. Their potential utility as diagnostics of both long-term (>10 years) and short-term atmospheric variability interests many who study them. Yet despite a diverse and rapidly growing database of satellite observations, there has been relatively little effort to quantitatively compare multiyear PMC observations from separate satellites [*Thomas*, 1995; *Shettle et al.*, 2002]. One challenge to this end is to find a standard for comparison between data sets and with global-scale climate models of the mesosphere.

[3] Year-to-year changes are clearly present in the PMC record. One source of change is the 11-year solar cycle, which drives temperature and water vapor variations in the upper mesosphere and can lead to variations in cloud brightness and occurrence frequency [*Thomas et al.*, 1991; *DeLand et al.*, 2003; *Siskind et al.*, 2005; *Hervig and Siskind*, 2006]. Furthermore, multiple data sets now indicate that the environment over Antarctica is less conducive to PMC formation than over the Arctic [*Thomas et al.*, 1991; *Bailey et al.*, 2005; *Hervig and Siskind*, 2006; *Petelina et al.*, 2006; *Wrotny and Russell*, 2006]. A quantitative assessment of these sources of temporal and spatial PMC variability would provide a crucial test for climate models.

[4] *Stevens et al.* [2005] suggested that by combining both the PMC frequency and brightness the total ice mass can be used as a standard of comparison. For observations of solar scattered light from PMCs, this approach requires information about the ice particle size distribution. The ice particle size distribution of PMCs has not yet been measured, but if a distribution function is assumed then its characteristics can be constrained either through remote observations or model results [*Thomas and McKay*, 1985; *Rusch et al.*, 1991; *Debrestian et al.*, 1997; *von Cossart et al.*, 1999; *von Savigny et al.*, 2005; *Rapp and Thomas*, 2006; *Karlsson and Rapp*, 2006]. In a companion paper by *Englert and Stevens* [2007] we showed that for mid-UV satellite observations of backscattered sunlight the ice content along the line of sight is insensitive to the characteristic size of the ice particles. Motivated by this appealing result, we herein determine the zonally integrated PMC mass and compare the results from two multiyear satellite data sets of mid-UV PMC observations.

[5] The suite of Solar Backscattered UltraViolet (SBUV) instruments has compiled the longest PMC database on record, stretching back to 1979. Its uninterrupted global coverage over more than 27 years makes it a useful data set for studying the effects of solar cycle variability on PMCs. The Student Nitric Oxide Explorer (SNOE) observed mid-UV solar scattered sunlight from PMCs for 6 years from 1998 to 2003, measuring a significantly higher PMC occurrence frequency than SBUV during this period because of its more favorable limb-viewing geometry. Such a viewing geometry significantly reduces the Rayleigh background contribution to the total signal, enhancing SNOE's

[1] Space Science Division, Naval Research Laboratory, Washington, D. C., USA.
[2] Science Systems and Applications, Inc., Lanham, Maryland, USA.
[3] Department of Electrical and Computer Engineering, Virginia Tech, Blacksburg, Virginia, USA.

Copyright 2007 by the American Geophysical Union.
0148-0227/07/2006JD007532

sensitivity to the PMC layer. The multiyear global coverage of SNOE is well suited for comparison with the SBUV data.

[6] The primary objectives of this work are (1) to compare the PMC ice mass observed by SNOE with that observed concurrently with SBUV, (2) to find the subset of bright SNOE PMCs that correspond to the SBUV observations, and (3) to determine the difference in the SBUV PMC mass at 70°N and 70°S.

[7] Section 2 presents a brief summary of our two data sets and an explanation of which observations are selected for this study. Section 3 describes how observed cloud frequencies are combined with the retrieved column ice mass to derive the PMC ice mass for both experiments. Section 4 compares the SBUV and SNOE PMC mass at 70°N and the SBUV PMC mass at 70°N and 70°S. Section 5 uses the SNOE PMC mass and the solar cycle variation derived for SBUV to derive the PMC ice mass as a function of latitude near mid-solar-cycle. The results from section 5 are used to compare with modeled PMC results from a global chemical/dynamical model in a companion paper [*Siskind et al.*, 2007].

2. PMC Observations

[8] PMC brightness and frequency vary not only with solar cycle, but can also vary with local time (LT) [*von Zahn et al.*, 1998; *Chu et al.*, 2003; *Fiedler et al.*, 2005; *Petelina et al.*, 2006; *Chu et al.*, 2006; *DeLand et al.*, 2007], latitude [e.g., *Olivero and Thomas*, 1986] and days relative to solstice (DRS) [e.g., *Thomas and Olivero*, 1989; *Bailey et al.*, 2005]. The influence of these effects can introduce biases to inferred long-term or hemispheric variations depending on when and where each experiment samples the polar summer mesosphere. We therefore only select portions of the SBUV and SNOE PMC data to remove or minimize these effects. Our selection criteria are discussed next.

2.1. SBUV Observations

[9] The SBUV and SBUV/2 PMC data set is composed of observations from six different satellites operating at various times since November 1978 [*DeLand et al.*, 2006]. SBUV PMC albedos are reported at 252.0 nm and the ice mass from one northern season of SBUV observations (1999) was derived by *Stevens et al.* [2005]. The SBUV data set has since been revised by *DeLand et al.* [2007] and we use their new PMC identification algorithm in our approach. The effect on the ice mass calculation is small and discussed further in section 5.

[10] Limb viewing PMC experiments typically observe cloud frequencies in excess of 80% poleward of 75° latitude [*Olivero and Thomas*, 1986; *Bailey et al.*, 2005, 2007]. Such high frequencies can lead to a negative bias in SBUV cloud frequencies and albedos because there are not enough clear air data to reliably specify the Earth's background albedo [*Deland et al.*, 2007]. We limit our most detailed comparisons that follow to latitudes 70 ± 2.5°N, which still provides enough PMC data for reliable statistics. SBUV results at other latitudes between 55 and 75°N will be presented in section 5.

[11] Each SBUV instrument typically observes PMCs near two different LT on each orbit: one on the ascending node and another on the descending node. At 70°N, these LT can be separated by several hours. We therefore sort the observations into 5° latitude bins and split these subsets into ascending and descending node data for each satellite and PMC season. The longest uninterrupted subset of SBUV data from all six satellites at 70 ± 2.5°N near a single time of day can be found by limiting observations to 11.4 ± 1.0 LT [*DeLand et al.*, 2007]. Average LT for each satellite and each year are shown in Figure 1a. Where there are two satellites measuring during one year, the average from each satellite is used to find the annual average. We then calculate the mean and standard deviation from the 27 annually averaged LT shown in Figure 1a.

[12] It is well known that the solar scattering angle for a mid-UV observation plays an important role in retrieving characteristics of the ice particle size distribution [e.g., *Thomas*, 1984; *Rapp and Thomas*, 2006; *Englert and Stevens*, 2007]. For our analysis, it is therefore important to assemble the data with as narrow a range of scattering angles as possible to avoid biases in the calculated PMC mass. Figure 1b shows the annually averaged solar scattering angles (θ) used for the derivation of the column ice mass from the observed PMC brightness. The solar scattering angle over all the years of Northern Hemisphere SBUV data considered herein is tightly constrained at 131 ± 2°, where the mean and standard deviation is calculated in the same way as for the LT in Figure 1a. We calculate the column ice mass using the specific solar scattering angle of each SBUV PMC observation before compiling the annual averages.

[13] To determine possible hemispheric asymmetries in the PMC mass, we also consider the SBUV data between 70 ± 2.5°S at nearly the same LT as used in the Northern Hemisphere. The annual variation of LT and solar scattering angle for these data are compared with the Northern Hemisphere data in Figures 2a and 2b. We note that the SBUV satellites do not necessarily sample the same LT in each hemisphere. Although there is some evidence in ground-based studies that the diurnal variation of PMCs near 70°S is different from that near 70°N and even from PMCs observed over the south pole [*von Zahn et al.*, 1998; *Chu et al.*, 2003, 2006], the implications of these results to multiyear mid-UV satellite observations of the PMC mass (i.e., both the frequency and the column ice mass) are not yet clear. For this study, we assume that observations at the same LT and latitude in each hemisphere affect the PMC mass in the same way.

[14] Figure 2a shows that although the coverage is more limited for the data in the south than in the north (the PMC seasons 1990–1991, 2001–2002, 2003–2004 and 2004–2005 are missing data at the LT indicated), the average LT is 12.9 ± 0.9 and similar to that used for the Northern Hemisphere. The corresponding scattering angles for the southern data are compared with those from the north in Figure 2b and the southern average is 125 ± 7°.

[15] Also indicated in Figures 1b and 2b are the days over which the data are averaged: −10 to 20 DRS. This time period is near the beginning of the PMC season that typically extends from about −20 to 60 DRS. The earlier portion of the season is selected because PMCs are illuminated for a longer time period during the day nearer to

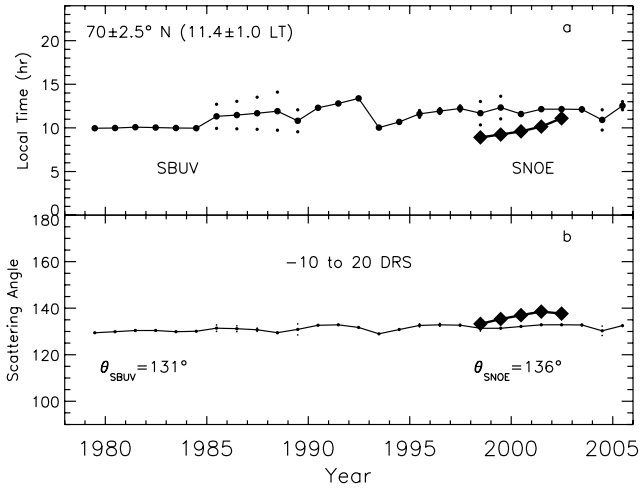

Figure 1. (a) Northern Hemisphere LT of the PMC observations considered herein. The SBUV data are assembled from instruments on six different satellites between 1979 and 2005. The thin line (with circles) indicates the SBUV data and the thick line (with diamonds) indicates the SNOE data. Where there is more than one SBUV instrument observing PMCs near the LT indicated during the same year (small circles), the data shown are averaged together for one representative measurement during that PMC season (large circles). (b) Solar scattering angle for the same observations represented in Figure 1a. The average SBUV scattering angle is indicated on the bottom left, and the average SNOE scattering angle is indicated in the bottom right. All data for each year are collected between −10 and 20 days relative to solstice (DRS).

solstice. Although the Earth's terminator does not affect the 70 ± 2.5° latitude region near midday, future comparisons of our results with other mid-UV solar backscatter observations at other LT may benefit from the selected period near solstice. We explore the sensitivity to our results using observations later in the season in section 4.1.

2.2. SNOE Observations

[16] SNOE was launched in February 1998 and reentered the Earth's atmosphere in December 2003. SNOE measured nitric oxide solar resonance fluorescence [*Barth et al.*, 2003] and solar scattered light from PMCs at two wavelengths: 215 nm and 237 nm. In the context of this work, both channels yield similar results and only the PMC data from 215 nm is used. SNOE observes PMCs with nearly uninterrupted coverage up to 82° latitude in both hemispheres [*Bailey et al.*, 2005]. The observations from the Southern Hemisphere were typically of forward scattered sunlight. This geometry severely limits our ability to infer the column ice mass from the PMC brightness because of greater sensitivity of the mass to the ice particle size distribution [*Englert and Stevens*, 2007]. We therefore use only the SNOE observations of backscattered light from PMCs in the Northern Hemisphere for this work.

[17] To be consistent with the LT of the SBUV measurements, we limit the SNOE data to that from the ascending node where the 5-year average LT is 9.8 at 70 ± 2.5°N. The SNOE LT drifted slightly higher during each PMC season from 1998 to 2002, as illustrated in Figure 1a. The pointing knowledge of SNOE degraded slightly in 2003 as the spacecraft neared the end of its lifetime and because knowledge of the solar scattering angle is critical to our analysis, these data are not included in this study. The SNOE scattering angles range between 133 and 137° at 70 ± 2.5°N from 1998 to 2002 and we use the 5-year average of 136° (indicated in Figure 1b) for analysis of all SNOE PMC observations. Since the SNOE data set is much shorter than the 27-year data set of SBUV, we directly compare the SNOE data only with SBUV data collected during the same 5 years.

3. Approach

[18] We employ two fundamental assumptions to infer and compare the PMC ice mass from SBUV and SNOE observations. First, we assume each PMC observation can be described with a Gaussian distribution of spherical water ice particles [*Berger and von Zahn*, 2002; *Rapp and Thomas*, 2006]. This is in slight contrast to our earlier work using one northern season of SBUV PMC data [*Stevens et al.*, 2005], where we used a lognormal distribution. Our second assumption is that the SBUV PMC observations are a bright subset of the SNOE observations. This is justified by the much lower occurrence frequency reported for SBUV over the same time period [*DeLand et al.*, 2003; *Bailey et al.*, 2005]. Our comparison therefore requires (1) a selection criterion for the SNOE data to create a SBUV equivalent subset of PMC observations and (2) the calculation of the SNOE and SBUV column ice mass from the reported cloud brightnesses. These two steps are discussed next.

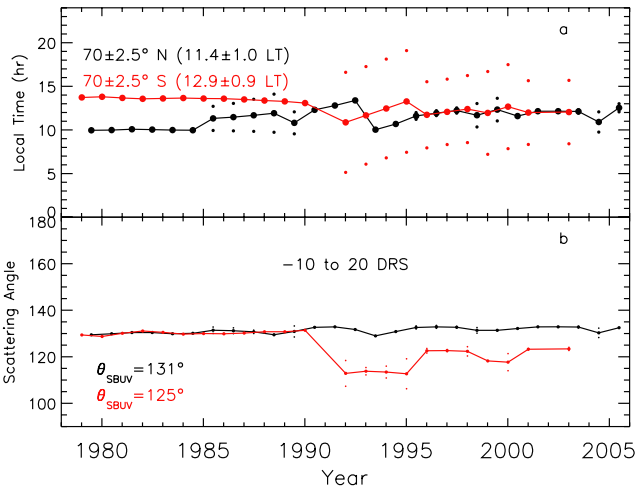

Figure 2. (a) SBUV LT comparison between Northern Hemisphere data (black, Figure 1) and Southern Hemisphere data (red) used in this work. (b) Solar scattering angle comparison for the Northern (black) and Southern Hemisphere data (red). The average scattering angles are indicated.

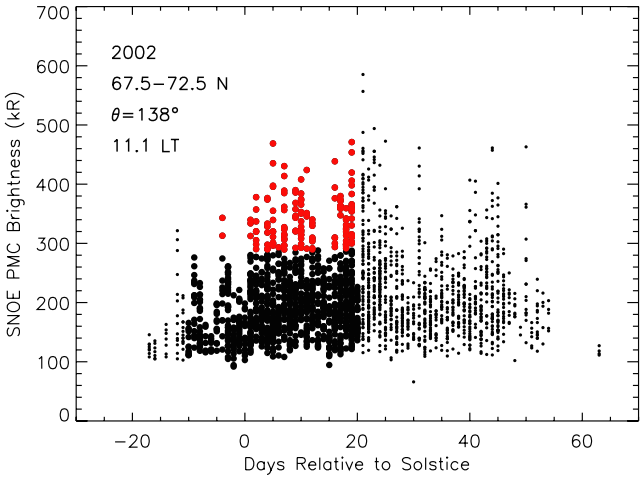

Figure 3. Example of one northern season (2002) of SNOE PMC data between 67.5 and 72.5°N. Each symbol represents a PMC observation. Large circles are the data over the time period used in this study. Large red circles are the brightest SNOE PMCs that on average match the SBUV cloud frequency and are therefore representative of the SBUV observations. These brightest PMCs are 10% of all SNOE PMC observations between −10 and 20 DRS.

3.1. Selection of the Brightest SNOE PMCs

[19] We determine the threshold brightness of the SNOE PMCs so that the average SNOE PMC occurrence frequency is the same as that from SBUV averaged over the same time period, latitudes and LT indicated in Figure 1. The threshold brightness under these conditions is 289 kiloRayleighs (kR), which corresponds to the brightest 10% of the SNOE cloud observations. Our approach is illustrated in Figure 3 for one season (2002) of SNOE PMC observations. Each symbol in Figure 3 represents one SNOE PMC observation, the larger circles (black and red) represent the PMCs detected over the portion of the season we consider and the larger red circles indicate the representative subset of SBUV PMCs. SNOE PMC frequencies are compared to SBUV occurrence frequencies for each year in Figure 4, with the frequency of

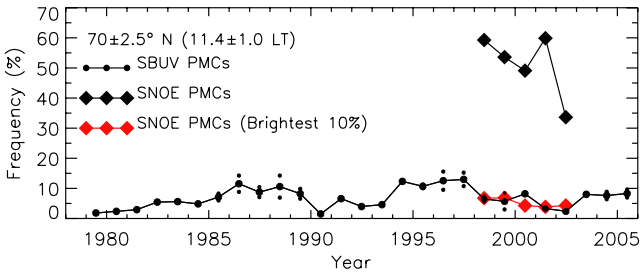

Figure 4. Northern Hemisphere PMC frequencies considered herein. SBUV LT are indicated, and the data are an average between −10 to 20 DRS. Average SNOE PMC frequencies each year between 1998–2002 are shown as the large diamonds. The frequency of the brightest PMCs from the SNOE data during this time period are shown as the red dashed line. The indicated threshold is set so that the average PMC frequency over the 5 years of SNOE data shown is the same over the same 5 years of SBUV data.

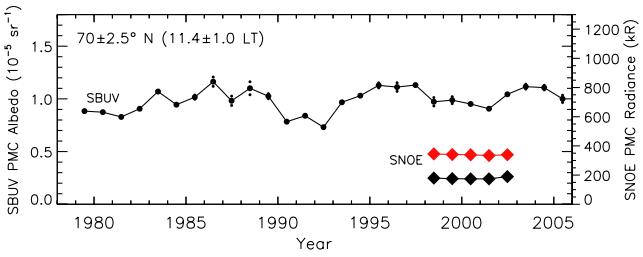

Figure 5. SBUV PMC albedos at 252.0 nm (circles) and SNOE PMC radiances at 215 nm (diamonds) analyzed herein for the ice mass column. The SNOE radiances are referenced to the right hand axis, and the average radiance of the brightest 10% of SNOE PMCs is shown in red.

clouds above the threshold shown in red. Note that in general, SNOE was operating near solar maximum so that the average SBUV frequency over this period is lower compared to the average over the 27 years of SBUV data shown. Note also that the daily frequency variation in Figure 3 and the annual variation in Figure 4 is not the same for the brightest clouds as it is for all the clouds. The annual variation of the brightest clouds is discussed further in section 4.1.

3.2. PMC Column Ice Mass

3.2.1. SBUV PMC Albedos

[20] Figure 5 shows SBUV annually averaged PMC albedos at 252.0 nm (units of 10^{-5} sr^{-1}). Because SBUV is nadir viewing, the relatively bright background albedo of the Earth must be identified in order to detect a PMC. The PMC signal is relatively small, on the order of 10% of the total albedo detected. The total albedo varies strongly with the solar zenith angle over each orbit [e.g., *Thomas et al.*, 1991; *DeLand et al.*, 2003]. The estimation of the total albedo is done using a polynomial fit through the observed signal and PMCs are identified as outliers above this signal. The uncertainty of a single PMC albedo at 70°N at a solar zenith angle of 40° is estimated to be near 23% by *DeLand et al.* [2007], where most of this uncertainty is statistical. The SBUV data used herein are compiled from a total of 3576 PMC observations over 27 years. The average number of observations included each year is therefore about 130, substantially reducing the uncertainty in the retrieved PMC brightness. We assume that the geophysical variations within each year are averaged out so that a single representative annual brightness may be derived. We therefore neglect the brightness uncertainty and carry only the larger uncertainty of the column ice mass that results from the limited constraints on the ice particle size distribution.

[21] To quantify the vertical column of ice from the SBUV albedos in Figure 5, we use Mie theory, which requires additional information on the ice particle size distribution. In a companion paper by *Englert and Stevens* [2007] we determined the variation in the vertical column ice mass using a range of reported characteristic radii (15–100 nm) and size distribution widths (10–20 nm). Figure 6 shows the annually averaged vertical column ice mass inferred using a reference radius (r_0) of 60 nm and width (σ_0) of 15 nm. The SBUV uncertainties in the computed column from the ambiguity in the size distribution

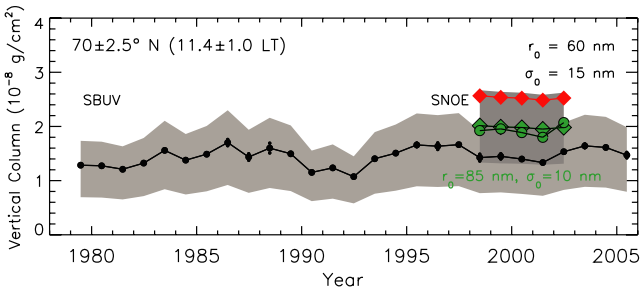

Figure 6. Annually averaged vertical mass column of ice for SBUV (circles) and SNOE (diamonds). For the nominal solution from both satellites, we use a characteristic particle radius of 60 nm and a Gaussian size distribution width of 15 nm. The SNOE slant ice mass column abundances have all been reduced by a factor of 97.1 for direct comparison with the vertical ice mass column abundances measured by SBUV (see text). The red symbols represent the brightest SNOE clouds for the nominal solution. The green symbols use a characteristic particle radius of 85 nm and distribution width of 10 nm. The shaded regions represent the uncertainty due to our selected radii (15 nm < r_0 < 100 nm) and widths (10 nm < σ_0 < 20 nm) of the particle size distribution.

characteristics are shown in Figure 6 (shaded area) and are +35%/−46% [*Englert and Stevens*, 2007].

3.2.2. SNOE PMC Brightnesses

[22] The annually averaged SNOE PMC brightnesses (in kR) between 1998 and 2002 are shown as the diamonds in Figure 5 and referenced to the scale on the right hand axis. Limiting the SNOE data to only the brightest 10% of observed clouds (see Figure 3) increases the annual average, and this subset of SNOE clouds is represented by the red line in Figure 5.

[23] We use the same particle size distribution for the brightest SNOE clouds (red) as for the SBUV clouds to calculate the vertical column shown in Figure 6. For the wavelength and solar scattering angle appropriate to the SNOE data shown in Figure 6, the uncertainties relative to the nominal solution are calculated from the same range of size distribution characteristics indicated in Figure 5 and are +4%/−48% [*Englert and Stevens*, 2007]. We have uniformly reduced the observed SNOE slant column ice mass by a single factor (97.1) for comparison with SBUV because of the longer viewing path through the PMC when viewed on the limb compared to when viewed in the nadir [*Thomas and McKay*, 1985; *Englert and Stevens*, 2007].

4. Results

4.1. SNOE Versus SBUV

[24] Figure 6 shows that the brightest 10% SNOE clouds yield an average column ice mass that is about 80% greater than that for SBUV clouds for the indicated characteristic size (60 nm) and distribution width (15 nm). Since the cloud frequencies are the same for the SNOE and SBUV data sets in Figure 6, this suggests that the arbitrarily chosen 60 nm is not the typical radius of the ice particles observed by both instruments. We also show a solution using a particle radius of 85 nm and a distribution width of 10 nm in green. In this example the SNOE and SBUV results are in much better agreement indicating that there are solutions within our parameter space that bring the data sets into agreement. Although the SNOE and SBUV data are in agreement within uncertainties, this comparison would benefit from more direct information on the characteristic radii.

[25] Using the approach of *Englert and Stevens* [2007], the PMC mass in Figure 7 is calculated by multiplying the SBUV and SNOE column abundances shown in Figure 6 by the occurrence frequencies in Figure 4 and by the area over which the observations are made (7.81×10^{16} cm^2). Between 1998 and 2002, we find that the more sensitive SNOE instrument is measuring at least a factor of three more PMC mass than SBUV for the conditions indicated in Figure 7. As in Figure 6, the solutions using the 10% brightest clouds from the SNOE data between −10 and 20 DRS are shown in red (r_0 = 60 nm). Because the start and end of the PMC season appears to vary from year to year [*DeLand et al.*, 2003], we considered how our solutions change when a different portion of the season is sampled. Between 0 and 35 DRS, we find that the average SNOE or SBUV PMC mass increases by 15% or less at all latitudes equatorward of 80°N.

[26] Although the agreement between the data sets in Figures 6 and 7 is good, there are year-to-year differences. One possibility is that the ambient conditions from one year to the next could yield slightly different sized ice particles. Without direct information on the particle radii or the ambient temperatures and water vapor during this time period, however, we cannot confirm this.

[27] To our knowledge, Figure 7 shows the first quantitative comparison of the PMC ice mass between two independent satellite data sets. Figure 7 also clearly shows a solar cycle variation in the PMC ice mass measured by SBUV of at least a factor of two. The strong solar cycle variation of the SBUV PMC occurrence frequency has been reported previously [e.g., *Thomas et al.*, 1991; *von Zahn et al.*, 2004], and is primarily driving the ice mass variation shown in Figure 7. The absolute value of the SBUV ice mass and the observed dynamic range over a solar cycle help to provide a new standard to which global models of ice formation can now be compared.

4.2. Northern Versus Southern PMCs

[28] Another of our objectives is to quantify the difference in the PMC mass between the Northern and Southern

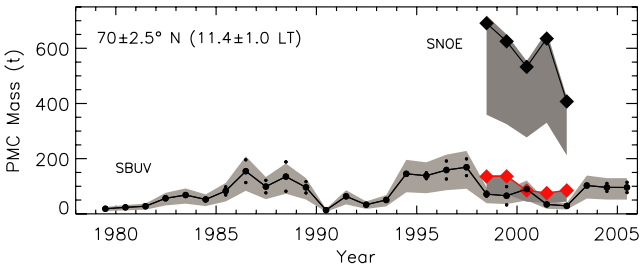

Figure 7. Annually averaged PMC ice mass. The shaded areas represent the uncertainty in the characteristics of the size distribution indicated in Figure 6. All solutions shown use the same size distribution as indicated in the upper right of Figure 6.

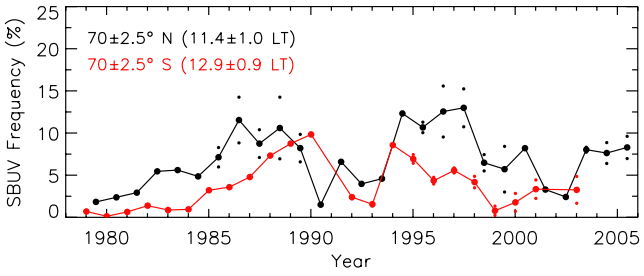

Figure 8. SBUV PMC occurrence frequencies for the indicated LT. Northern Hemisphere results (in black) are reproduced from Figure 4 for comparison with Southern Hemisphere results (in red).

Hemisphere. As indicated earlier, SNOE typically measures forward scattered solar radiation in the Southern Hemisphere [*Bailey et al.*, 2005], making the PMC ice mass far more sensitive to small variations in the particle size distribution [*Englert and Stevens*, 2007]. We therefore avoid using SNOE data from the Southern Hemisphere in this study and limit our analysis of hemispheric asymmetries exclusively to SBUV data.

[29] Figure 8 shows the SBUV cloud frequencies from the north and south for nearly the same LT and latitude over the 27-year data set. For the same years over which there is data from both hemispheres at the LT indicated in Figure 8, Southern Hemisphere PMCs occur on average 47% less frequently in the south (red) than in the north (black). Lower frequencies in the south are generally consistent with previous work. *Wrotny and Russell* [2006] found that PMCs were 50% less frequent in the south between 55 and 70° latitude using satellite data from the Halogen Occultation Experiment (HALOE) obtained between 1992 and 2005. *Petelina et al.* [2006] reported that PMCs were about 40% less frequent in the south compared to the north using observations from the Optical Spectrograph and Infrared Imager System (OSIRIS) PMC observations between 2001 and 2003 and 60–82° latitude. *Bailey et al.* [2007] reported interhemispheric differences from special SNOE operations in 2000–2001, during which solar scattered light from PMCs were observed at similar scattering angles. These observations showed that between 60 and 80° latitude, southern PMCs were about 30% less frequent than northern PMCs. We note that year-to-year frequency variations in Figure 8 are large in both hemispheres so that averages over

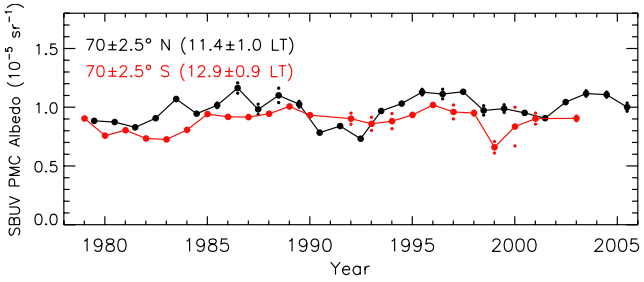

Figure 9. SBUV PMC albedos at 252.0 nm from opposite hemispheres analyzed herein. The 70°N albedos are reproduced from Figure 5 for comparison.

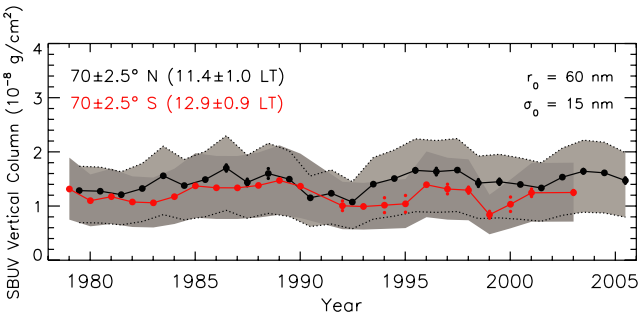

Figure 10. Vertical water ice column inferred from SBUV PMC data in opposite hemispheres. Characteristics of the particle size distribution are indicated in the upper right and are the same for both hemispheres.

shorter durations using instruments with different sensitivities can easily yield different results.

[30] Dimmer clouds have been reported in solar backscattered PMC data in the south when compared to the north [*Olivero and Thomas*, 1986; *Thomas et al.*, 1991; *DeLand et al.*, 2006; *Petelina et al.*, 2006]. Figure 9 shows the annual variation of the SBUV albedos at 70 ± 2.5°S. The albedo at 252.0 nm at 70 ± 2.5°N (Figure 5) is overplotted for comparison. Northern clouds are generally brighter, but the determination of the ice content requires consideration of both the solar scattering angle (Figure 2b) and the relevant particle size distribution.

[31] Figure 10 shows a comparison of the vertical column ice mass in each hemisphere. The indicated characteristics of the Gaussian size distribution are the same as those used for the Northern Hemisphere. We propagate the uncertainty shown by the shaded areas in Figure 10 directly to the PMC mass calculation shown in Figure 11. Although the average Northern Hemisphere column is 20% larger than that in the south, the uncertainties in both the size and width of the particle size distributions in both hemispheres are too large to draw such a general conclusion with these SBUV data. To help constrain the derived hemispheric asymmetry of the column ice mass, we consider additional PMC observations by HALOE. HALOE performs a direct measurement of the volume of ice along the line of sight and unlike SBUV does not require additional information on the particle size distribution to determine the column ice mass. HALOE data show that northern PMCs had 30% greater extinction than southern PMCs [*Hervig and Siskind*, 2006; *Wrotny and Russell*, 2006]. This indicates therefore that northern clouds are 30% more massive at nearly the same latitudes as considered here, in general agreement with the nominal solutions in Figure 10. If we use the HALOE result, we find the best solution is that the northern PMC mass is a factor of 2.4 greater than the southern PMC mass at 70 ± 2.5° latitude. This difference is primarily driven by the factor of two difference in the PMC frequency in Figure 8.

5. Discussion

[32] Figure 7 shows that the less sensitive SBUV instrument yields a severe underestimate of the total mesospheric ice mass near 70°N. We now extend the comparison to other latitudes. Figure 12 shows the PMC mass derived from

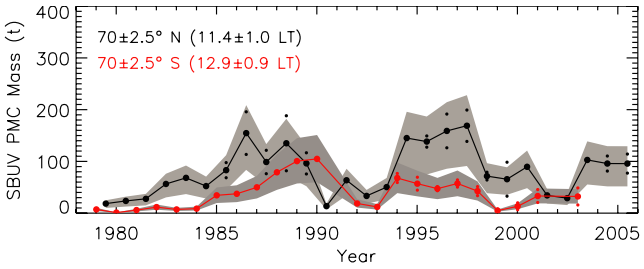

Figure 11. Comparison of the total PMC ice mass observed by SBUV in the Northern and Southern hemispheres.

SNOE and SBUV observations at five different latitudes between 55 and 75°N in 5° increments. The LTs indicated in Figure 12 (9.2–11.8) are determined from the observations at each latitude between 55 and 75°N. The lower LT limit is from the SNOE 5-year average near 75°N and the upper limit is from the SBUV 27-year average near 55°N.

[33] In Figure 12 we use the same range of Gaussian size distribution characteristics (r_0 = 15–100 nm; σ_0 = 10–20 nm) at all latitudes shown and for each data set. We use the scattering angle specific to each latitude to derive the PMC mass from the average cloud brightness. The average solar scattering angle for the SNOE data varies between 122 and 148° from 55 to 80°N and the scattering angle for the SBUV data varies between 144 and 126° from 55 to 75°N. The relative range of solutions shown by the shaded area for each set of observations is derived from the solutions at 70 ± 2.5°N. The SBUV ice mass derived at latitudes poleward of 75°N is less certain and not shown because of the increased difficulty in defining the Earth's mid-UV albedo, as discussed earlier. The mass reduction nearer to the pole in the SNOE data is due to the smaller surface area for that region.

[34] The 27-year average SBUV mass can be placed in the context of previous work by *Stevens et al.* [2005], who derived the PMC mass from one season of SBUV observations near mid-solar-cycle. In that work, observations from the northern summer of 1999 showed an average PMC mass of ~70 t/5° latitude at 70°N and 4.7 LT. SBUV PMC frequencies are greater in the early morning by up to a factor of two compared to late morning [*DeLand et al.*, 2007], in general agreement with ground based observations [*Fiedler et al.*, 2005]. Revisions in the PMC mass due to the new SBUV retrieval algorithm [*DeLand et al.*, 2007], the characteristics of the size distribution [*Englert and Stevens*, 2007] and the days over which the average PMC mass was defined (section 4.1) all contribute less than the LT effect. When adjusted to late morning conditions near 70°N, this mass is ~35–70 t/5°, generally consistent with the result in Figure 12.

[35] Since SNOE operated near solar maximum conditions, the SNOE data in Figure 12 have been scaled upward to represent mid-solar-cycle conditions for comparison with the 27-year average of SBUV data shown. For this scaling, we ratio the 27-year average SBUV PMC mass to that derived from SBUV during the SNOE observations for each 5° latitude bin. Thus we assume that the solar cycle response of the ice particles observed by SBUV and SNOE is the same. The upward scaling to the SNOE data ranges between 21% near 55°N to 42% near 75°N.

[36] Although SNOE detects at least three times more mass than SBUV, there is likely to be a small portion of the cloud population to which it is not sensitive. We note, however, that using observations of backscattered sunlight from PMCs in the Northern Hemisphere *Bailey et al.* [2005] reported the daily averaged PMC frequency to be up to 100% near 80° latitude. We therefore regard any contribution to the total PMC mass by undetectable ice particles to be small compared to the uncertainties in the size distribution shown in Figure 7. Therefore we do not include an estimate for the mass of the clouds below the SNOE detection threshold in Figure 12.

[37] In addition to quantifying the underestimate of the PMC mass in the polar summer by SBUV, Figure 12 serves to illustrate that the difference between the SNOE and SBUV PMC mass with latitude. The difference is most pronounced at the highest latitudes (65–75°N), whereas the PMC mass is nearly the same for both SNOE and SBUV at the lower latitudes (55–60°N). The SBUV algorithm that identifies a PMC becomes more uncertain at lower latitudes. Therefore we cannot say whether the agreement with SNOE at lower latitudes is due to geophysical variations in the ice particle properties.

6. Summary

[38] We have compared the PMC ice mass at 70 ± 2.5°N from two different multiyear satellite data sets: SNOE and SBUV. We assume that the ice particles are spherical and their size distribution may be adequately described for each set of observations by a Gaussian with a representative radius and width. We find that on average SNOE measures at least three times more mass than SBUV because of its greater sensitivity. By limiting the comparison to the brightest 10% of PMCs from SNOE so that the occurrence frequency is the same for both data sets, we directly

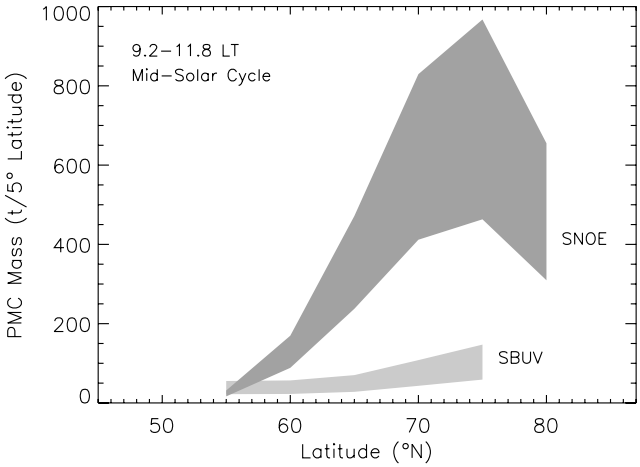

Figure 12. Ice mass between 55 and 80°N inferred from SNOE and SBUV data. Data are averaged between −10 and 20 DRS and in 5° latitude bins between the local times indicated. Uncertainties are from the range of size distribution characteristics considered and shown in Figures 6 and 10.

compare the SNOE PMC mass with the SBUV PMC mass for the same latitude, years and LT. We find good agreement between SNOE and SBUV within current uncertainties in the ice particle size distribution. Finally, by selecting SBUV PMC data from the same latitudes and LT in both hemispheres, we find that the SBUV PMC ice mass at 70 ± 2.5°N is a factor of 2.4 times larger than at 70 ± 2.5°S.

[39] Future estimates of the PMC ice mass from satellite measurements would benefit from tighter constraints on the ice particle size distribution relevant to the observations. The SBUV PMC data set is the longest satellite data set on record, so our conclusions on the absolute PMC mass, its hemispheric asymmetry and its variation with latitude pose challenges to future global modeling studies of long-term PMC variations.

[40] **Acknowledgments.** This work was supported by the Sun Earth Connection Guest Investigator Program in the NASA Science Mission Directorate. We thank D. W. Rusch for several helpful discussions on the analysis of the SNOE data.

References

Bailey, S. M., A. W. Merkel, G. E. Thomas, and J. N. Carstens (2005), Observations of polar mesospheric clouds by the Student Nitric Oxide Explorer, *J. Geophys. Res.*, *110*, D13203, doi:10.1029/2004JD005422.

Bailey, S. M., A. W. Merkel, G. E. Thomas, D. W. Rusch (2007), Interhemispheric differences in polar mesospheric cloud morphology observed by the Student Nitric Oxide Explorer, *J. Atmos. Sol. Terr. Phys.*, in press.

Barth, C. A., K. D. Mankoff, S. M. Bailey, and S. C. Solomon (2003), Global observations of nitric oxide in the thermosphere, *J. Geophys. Res.*, *108*(A1), 1027, doi:10.1029/2002JA009458.

Berger, U., and U. von Zahn (2002), Icy particles in the summer mesopause region: Three-dimensional modeling of their environment and two-dimensional modeling of their transport, *J. Geophys. Res.*, *107*(A11), 1366, doi:10.1029/2001JA000316.

Chu, X., C. S. Gardner, and R. G. Roble (2003), Lidar studies of interannual, seasonal, and diurnal variations of polar mesospheric clouds at the South Pole, *J. Geophys. Res.*, *108*(D8), 8447, doi:10.1029/2002JD002524.

Chu, X., P. J. Espy, G. J. Nott, J. C. Diettrich, and C. S. Gardner (2006), Polar mesospheric clouds observed by an iron Boltzmann lidar at Rothera (67.5°S, 68.0°W), Antarctica from 2002 to 2005: Properties and implications, *J. Geophys. Res.*, *111*, D20213, doi:10.1029/2006JD007086.

Debrestian, D. J., et al. (1997), An analysis of POAM II solar occultation observations of polar mesospheric clouds in the Southern Hemisphere, *J. Geophys. Res.*, *102*(D2), 1971–1981.

DeLand, M. T., E. P. Shettle, G. E. Thomas, and J. J. Olivero (2003), Solar backscattered ultraviolet (SBUV) observations of polar mesospheric clouds (PMCs) over two solar cycles, *J. Geophys. Res.*, *108*(D8), 8445, doi:10.1029/2002JD002398.

DeLand, M. T., E. P. Shettle, G. E. Thomas, and J. J. Olivero (2006), A quarter-century of satellite polar mesospheric cloud observations, *J. Atmos. Sol. Terr. Phys.*, *68*, 9–29.

DeLand, M. T., E. P. Shettle, G. E. Thomas, and J. J. Olivero (2007), Latitude-dependent long-term variations in polar mesospheric clouds from SBUV version 3 PMC data, *J. Geophys. Res.*, doi:10.1029/2006JD007857, in press.

Englert, C. R., and M. H. Stevens (2007), Polar mesospheric cloud mass and the ice budget: 1. Quantitative interpretation of mid-UV cloud brightness observations, *J. Geophys. Res.*, *112*, D08204, doi:10.1029/2006JD007533.

Fiedler, J., G. Baumgarten, and G. von Cossart (2005), Mean diurnal variations of noctilucent clouds during 7 years of lidar observations at ALOMAR, *Ann. Geophys.*, *23*, 1175–1181.

Hervig, M., and D. Siskind (2006), Decadal and inter-hemispheric variability in polar mesospheric clouds, water vapor, and temperature, *J. Atmos. Sol. Terr. Phys.*, *68*, 30–41.

Karlsson, B., and M. Rapp (2006), Latitudinal dependence of noctilucent cloud growth, *Geophys. Res. Lett.*, *33*, L11812, doi:10.1029/2006GL025805.

Olivero, J. J., and G. E. Thomas (1986), Climatology of polar mesospheric clouds, *J. Atmos. Sci.*, *43*, 1263–1274.

Petelina, S. V., D. A. Degenstein, E. J. Llewellen, and N. D. Lloyd (2006), Correlation of PMC relative brightness and altitudes observed by Odin/OSIRIS in the Northern Hemisphere in 2002–2003, *J. Atmos. Sol. Terr. Phys.*, *68*, 56–64.

Rapp, M., and G. E. Thomas (2006), Modeling the microphysics of mesospheric ice particles—Assessment of current capabilities and basic sensitivities, *J. Atmos. Sol. Terr. Phys.*, *68*, 715–744.

Rusch, D. W., G. E. Thomas, and E. J. Jensen (1991), Particle size distributions in polar mesospheric clouds derived from Solar Mesosphere Explorer measurements, *J. Geophys. Res.*, *96*(D7), 12,933–12,939.

Shettle, E. P., G. E. Thomas, J. J. Olivero, W. F. J. Evans, D. J. Debrestian, and L. Chardon (2002), Three-satellite comparison of polar mesospheric clouds: Evidence for long-term change, *J. Geophys. Res.*, *107*(D12), 4134, doi:10.1029/2001JD000668.

Siskind, D. E., M. H. Stevens, and C. R. Englert (2005), A model study of global variability in mesospheric cloudiness, *J. Atmos. Sol. Terr. Phys.*, *67*, 501–513.

Siskind, D. E., M. Hervig, J. Gumbel, and M. H. Stevens (2007), Polar mesospheric cloud mass and the ice budget: 3. Application of a coupled ice-chemistry-dynamics model and comparison with observations, *J. Geophys. Res.*, *112*, D08303, doi:10.1029/2006JD007499.

Stevens, M. H., C. R. Englert, M. T. DeLand, and M. Hervig (2005), The polar mesospheric cloud mass in the Arctic summer, *J. Geophys. Res.*, *110*, A02306, doi:10.1029/2004JA010566.

Thomas, G. E. (1984), Solar Mesosphere Explorer measurements of polar mesospheric clouds (noctilucent clouds), *J. Atmos. Terr. Phys.*, *46*(9), 819–824.

Thomas, G. E. (1995), Climatology of polar mesospheric clouds: Interannual variability and implications for long-term trends, in *The Upper Mesosphere and Lower Thermosphere: A Review of Experiment and Theory*, *Geophys. Monogr. Ser.*, vol. 87, edited by R. M. Johnson and T. L. Killeen, pp. 185–200, AGU, Washington, D. C.

Thomas, G. E., and C. P. McKay (1985), On the mean particle size and water content of polar mesospheric clouds, *Planet. Space Sci.*, *33*(10), 1209–1224.

Thomas, G. E., and J. J. Olivero (1989), Climatology of polar mesospheric clouds: 2. Further analysis of Solar Mesospheric Explorer data, *J. Geophys. Res.*, *94*(D12), 14,673–14,681.

Thomas, G. E., R. D. McPeters, and E. J. Jensen (1991), Satellite observations of polar mesospheric clouds by the Solar Backscattered Ultraviolet spectral radiometer: Evidence of a solar cycle dependence, *J. Geophys. Res.*, *96*(D1), 927–939.

von Cossart, G., J. Fielder, and U. von Zahn (1999), Size distributions of NLC particles as determined from 3-color observations of NLC by ground-based lidar, *Geophys. Res. Lett.*, *26*(11), 1513–1516.

von Savigny, C., et al. (2005), Vertical variation of NLC particle sizes retrieved from Odin/OSIRIS limb scattering observations, *Geophys. Res. Lett.*, *32*, L07806, doi:10.1029/2004GL021982.

von Zahn, U., G. von Cossart, and J. Fiedler (1998), Tidal variations of noctilucent clouds measured at 69°N latitude by groundbased lidar, *Geophys. Res. Lett.*, *25*(9), 1289–1292.

von Zahn, U., G. Baumgarten, U. Berger, and P. Hartogh (2004), Noctilucent clouds and the mesospheric water vapour: The past decade, *Atmos. Chem. Phys.*, *4*, 2449–2464.

Wrotny, J. E., and J. M. Russell III (2006), Interhemispheric differences in polar mesospheric clouds observed by the HALOE instrument, *J. Atmos. Sol. Terr. Phys.*, *68*, 1352–1369.

S. M. Bailey, Department of Electrical and Computer Engineering, Virginia Tech, Blacksburg, VA 24061, USA.

M. T. DeLand, Science Systems and Applications, Inc., Lanham, MD 20706, USA.

C. R. Englert and M. H. Stevens, Space Science Division, Naval Research Laboratory, Washington, DC 20375, USA. (michael.stevens@nrl.navy.mil)